A Study of the Effect of Taheri Consciousness Bond Field on the Mechanical Crushing of Silica Particles

Bahareh Kazazi[1*], Mohammad Ali Taheri[2]

1. Civil Engineering, CEO of Hoobe Construction Company, Tehran, Iran.

2. Sciencefact R&D Department, Cosmointel Inc. Research Center, Ontario, Canada.

* Corresponding author:

Bahareh Kazazi
Civil Engineering, CEO of Hoobe Construction Company, Tehran, Iran.

Email: baharkazazi@gmail.com

The First Journal in T-Consciousness Research
Journal of Cosmo Intel
120

ABSTRACT

One of the materials used in various industries is silica. To achieve silica of different dimensions, mainly the method of crushing silica minerals is utilized. Taheri Consciousness Fields (TCFs) were founded and introduced by Mohammad Ali Taheri as new Fields more than four decades ago. These Fields are immaterial and non-energetic, so they have no quantity, but they have direct effects on matter and energy. In other words, although TCFs are not directly measurable, we can indirectly study their effects with various controlled experiments. Therefore, the study of the effect of the Consciousness Bond Field, as one of the Fields, on the process of crushing pure silica is the subject of this study. Initially, relatively pure silica grain (98% purity) was prepared. 10 samples were prepared, 5 of which were put under Consciousness Bond Field. Each sample included 50 grams' of silica in a titanium mechanical mill with 4 bullets of size 20, 20 bullets of size 15, 20 bullets of size 10, and 8 bullets of size 12. They were all under the same thermal and physical conditions and were milled alternately XRD (X-ray diffraction), DLS (Dynamic Light-Scattering), Zeta Potential (Electro-kinetic Potential), once with ultrasonic bath, once without ultrasonic, TEM (Transmission Electron–Microscopy), and SEM (Scanning Electron Microscopy) tests were done on the samples. It was found that in the samples under TCF, the strain of the crystalline lattice decreased, the distribution of the particles was more uniform, and the size of the smallest particles decreased. The electric charge of the particles' surface immediately after milling was dispersed in the samples under the TCF and finally, the resultant charge of the particles' surface neutralized each other after the use of an ultrasonic bath the TCF effect was reduced, and the surface load was measurable.

Keywords: Mechanical milling, crushing, silica, Consciousness Bond Field, Taheri Consciousness Fields

INTRODUCTION

One of the materials used in various industries is silica. Silica is not very usable as a crystal or mineral and for better performance, it needs to be reduced to smaller dimensions and in the best conditions nanometers in different ways. One of the most cost-effective methods is to mill silica rocks. The way of milling can break the material to nanomaterial dimensions. For this purpose, it is necessary for about 50% of the crystal dimensions of the particles to be between 1 and 100 nm [1]. Since the main purpose of this study was not to create nanomaterials but to investigate the effect of the immaterial factor of the Consciousness Field on the mechanical work process, so the test method was chosen to control the adhesion of the material to the wall and only the effect of the Consciousness Field on the mechanical work was studied.

One of the materials used in various industries is silica. Silica is not very usable as a crystal or mineral and for better performance, it needs to be reduced to smaller dimensions and in the best conditions nanometers in different ways. One of the most cost-effective methods is to mill silica rocks. The way of milling can break the material to nanomaterial dimensions. For this purpose, it is necessary for about 50% of the crystal dimensions of the particles to be between 1 and 100 nm [1]. Since the main purpose of this study was not to create nanomaterials but to investigate the effect of the immaterial factor of the Consciousness Field on the mechanical work process, so the test method was chosen to control the adhesion of the material to the wall and only the effect of the Consciousness Field on the mechanical work was studied.

The nature of consciousness and its place in science has received much attention in the current century. Many philosophical and scientific theories have been proposed in this area. In the1980s, Mohammad Ali Taheri introduced novel fields with a non-material/non-energetic nature named Taheri Consciousness Fields (TCFs). In this perspective, T-Consciousness is one of the three existing elements of the universe apart from matter and energy. According to this theory, there are various TCFs with different functions, which are the subcategories of a networked universal internet called the Cosmic Consciousness Network (CCN). The major difference between the theory of TCFs and other theoretical concepts about consciousness is related to the practical application of the TCFs. TCFs can be applied to all living and non-living creatures, including plants, animals, microorganisms, materials, etc.

Mohammad Ali Taheri, the founder of Erfan Keyhani Halqeh, a school of thought, introduced a new science in 2020 as a branch of this school. He coined the term Sciencefact for this new science because it utilizes scientific investigations to prove the existence of T-Consciousness as an irrefutable phenomenon and a fact. Although science focuses solely on the study of matter and energy and Sciencefact, by contrast, explores the effects of the [non-material/non-energetic] TCFs, Sciencefact has provided a common ground between the two by conducting reproducible laboratory experiments in various scientific fields, and it has used the scientific approach in proving TCFs.

The influence of the TCFs begins with the Connection between CCN as the Whole Taheri Consciousness of the universe and the subjects of study as a part. This Connection called “Ettesal” is established by a certified and trained individual who has been entrusted with the TCFs. The human mind has an intermediary role (Announcer) which plays a part by fleeting attention to the subject of study and then the main achievement obtained as a result of the effects of the TCFs. These Fields

cannot be directly measured by science, but it is possible to investigate their effects on various subjects through reproducible laboratory experiments.

The research methodology in the study of T-Consciousness has been founded on the process of Assumption, Argument, and Proof, in which the basic Assumption is: The Cosmos was formed by a third element called T-Consciousness that is different from matter and energy.

The Argument: The existence of TCFs can be demonstrated by its effects on matter and energy (e.g., humans, animals, plants, microorganisms, cells, materials, etc.)

The Proof: is the scientific verification of the effects of TCFs on matter and energy (according to the Argument) through various reproducible scientific experiments.

Accordingly, to investigate and verify the existence, effects, and mechanisms of TCFs, the following five research phases (Phases 0 through 4), and the aims of each phase are outlined below.

Phase-0 studies aim to prove the existence of TCFs by observing their effects. The nature of T-Consciousness and what it is will not be addressed in this phase. Phase-1 explores the varied effects of different TCFs. Phase-2 examines the reason behind the varied effects of these fields. Phase-3 investigates the mechanism of TCFs effects on matter and energy. Finally, Phase-4 draws significant conclusions, particularly with regard to the mind and memory of matter and their relation to the T-Consciousness, etc. [2-5]

Method and materials

Materials

Initially, relatively pure silica grain (98% purity) was obtained from a mineral that had previously been subjected to quality control. 10 samples were prepared, 5 of which were put under the Consciousness Field. Each sample included 50 grams of silica in a titanium mill with 4 bullets of size 20, 20 bullets of size 15, 20 bullets of size 10, and 8 bullets of size 12 under the following conditions: Time: 3hr; 15 'on; rest: 5'; rate: 400 rpm; ball/(material):10/1

And the same heat and physical conditions were applied to all samples, and they have milled alternately.

Table 1 . Groups synthesized simultaneously and under exactly the same conditions.

Names of the Control Samples	1	2	3	4	5
Names of the Samples under the TCF	H	I	J	K	L

Figure 1 - Schematic drawing of the concrete cracking process by alkali-silica reaction

Application of Taheri Consciousness Fields

One of the introduced TCFs, is called the Consciousness Bond Field and was applied to the samples according to the protocols regulated by the COSMOintel research center (www.COSMOintel.com). A request for Connection to the CCN to utilize TCFs can be placed through the COSMOintel website in the "Assign Announcement" section. This access is available for everyone at no cost. In order to study and experience this Connection, the researchers can register on the website at any time in order to report the experiment to the COSMOintel research center. Certain details of the experiment must be provided to the center; for example, the characteristics or number and name of samples and controls must be specified. This entire experiment was carried out as a double-blind method where lab technicians were completely unaware of the TCFs.

Analysis Method

XRD (X-ray diffraction) according to standard BSIBS En139251-2 and Generator Settings: 40 mA, 40 kV, Anode Material: Cu, Step Size [°2Th.]: 0.0260.

TEM (Transmission electron microscopy) by Zeiss EM900

Zeta Potential (Electro-kinetic Potential) and DLS (Dynamic Light Scattering) Were done by (Malvern-Nano ZS (red badge) ZEN 3600) and Dispersant Name: Water; Dispersant IR:1.336; Viscosity (Cp):0.8872; Dispersant Dielectric Constant:78.5

And zeta-potential re-testing by applying a 50 Hz ultrasonic with Bandelin device for 5 hours. All analyzes were done according to ISO 7-1502-3001 at 25 ℃, 19% RH humidity, and 1atm pressure. And finally, SEM (Scanning electron microscopy) was done on all samples.

Results and discussion

XRD (X-ray diffraction)

To identify the phases of matter Highscore plus X'Pert software was used. The results are presented below.

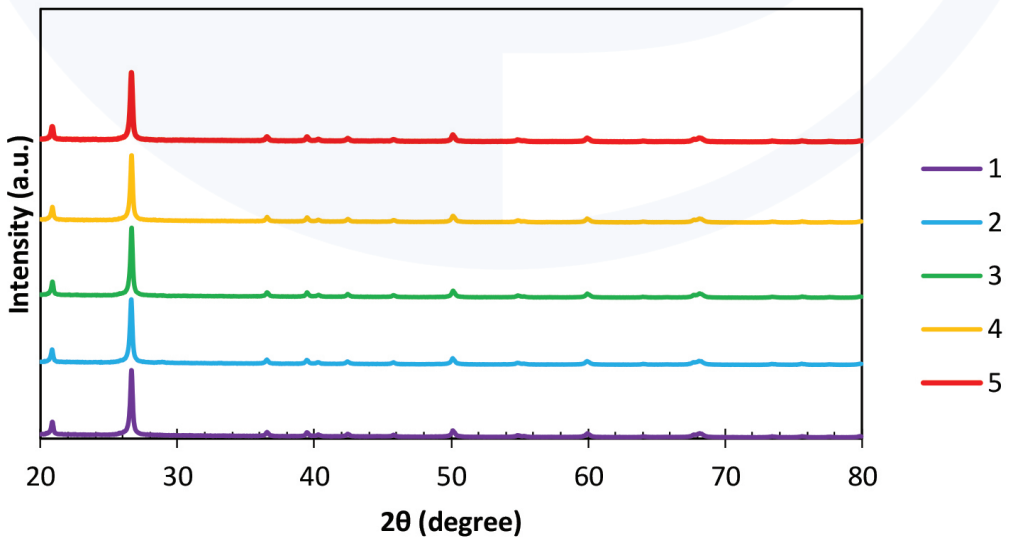

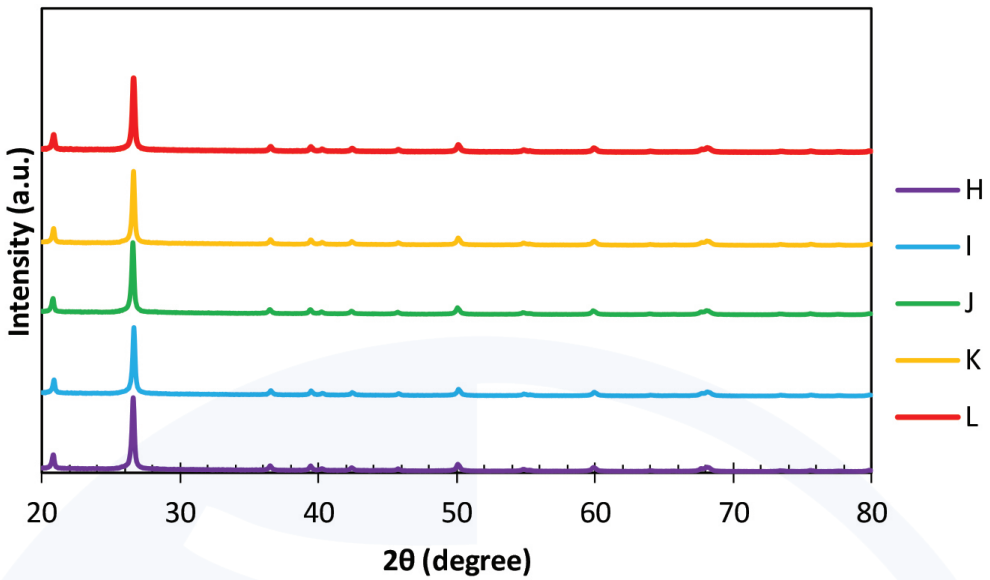

Figure 2 - X-ray diffraction pattern of the sample relating to SiO2 samples

According to Figure 2 and by matching this diffraction pattern with the reference diffraction patterns, it was determined that this diffraction pattern related to the quartz phase (SiO2) with the reference code JCPDS No. 01-078-1252 had a hexagonal crystal structure and space group P3121. In this structure, diffraction plates (100), (011), (110), (102), (200), (021), (112), (202), (121), (212) and (203) were respectively Observed at angles of 20.8 °, 26.6 °, 36.5 °, 39.4 °, 42.4 °, 45.7 °, 50.1 °, 54.8 °, 59.9 °, 67.6 ° and 68.1 °. These results showed that no phase other than quartz was observed in these samples.

To accurately examine the small values obtained from the XRD test related to these samples, the Rietveld method was used using MAUD software. This method is a technique proposed by Hugo Rietveld for use in the identification of crystalline materials. In this technique, the height, width, and position of each peak in its X-ray diffraction pattern can be used to determine many structural aspects of the material. Rietveld technique uses the least-squares method to better fit the theoretical values on the measured values [6,7]. The results of this method are shown in Table 2.

Table 2 . Quantitative results of Rietveld method XRD test

Samples	a (Angstrom)	c (Angstrom)	Crystallite Size (nm)	Micro strain
1	4.918	5.410	69.639	4.10×10^{-7}
2	4.919	5.410	69.640	3.77×10^{-7}
3	4.919	5.411	69.638	3.99×10^{-7}
4	4.919	5.411	69.640	5.99×10^{-7}
5	4.919	5.410	69.640	4.76×10^{-7}
H	4.918	5.410	69.639	4.10×10^{-7}
I	4.919	5.411	69.640	1.23×10^{-8}
J	4.918	5.410	69.640	1.74×10^{-10}
K	4.918	5.411	69.640	3.37×10^{-10}
L	4.919	5.411	70.916	7.99×10^{-9}

According to the results reported in Table 2, the values of the grid parameter in the hexagonal structure were equal to 4.918 to 4.919 angstroms for the horizontal grid parameter (a) and 5.410 to 5.411 angstroms for the vertical grid parameter (c). These values indicate that the grid parameter values are almost equal in all samples and the variables have no effect on the crystal structure of the material. Also, the size of the crystallite obtained for different samples was very close to each other and only the crystallite size of the sample (L) was slightly larger than the other samples. In addition, the micro-strain in all samples was very small and in the range of less than 10 to the negative power of 6. This indicates that there was no internal stress in the crystal structure of the samples and the grid distortion in the obtained crystal structures was very small. According to these results, the micro-strain and as a result, the distortion of the crystal grid in the samples under the CF was less than in the control samples.

Table 3 . Percentage of changes of mean micro-strain

	Under CF	Control	Percent of changes%
Mean micro-strain	8.616×10^{-8}	4.522×10^{-7}	-80.946

DLS and Zeta potential

Dynamic Light Scattering (DLS) is a physical method used to determine the distribution of particles in solutions and suspensions. This non-destructive and fast method is used to determine the particle size in the range of a few nanometers to microns. In this method, the scattered light by the nanoparticles in the suspension changes with time, which can be related to the particle diameter. What is obtained in this test for the particle size is the hydrodynamic diameter of the particles and, therefore, the values obtained in this test are different from the values obtained from the microscopic test [8].

DLS and zeta potential tests have been used to investigate the hydrodynamic particle size as well as the condition of the particles within the colloid. Figure 3 shows the particle size distribution histograms for the samples.

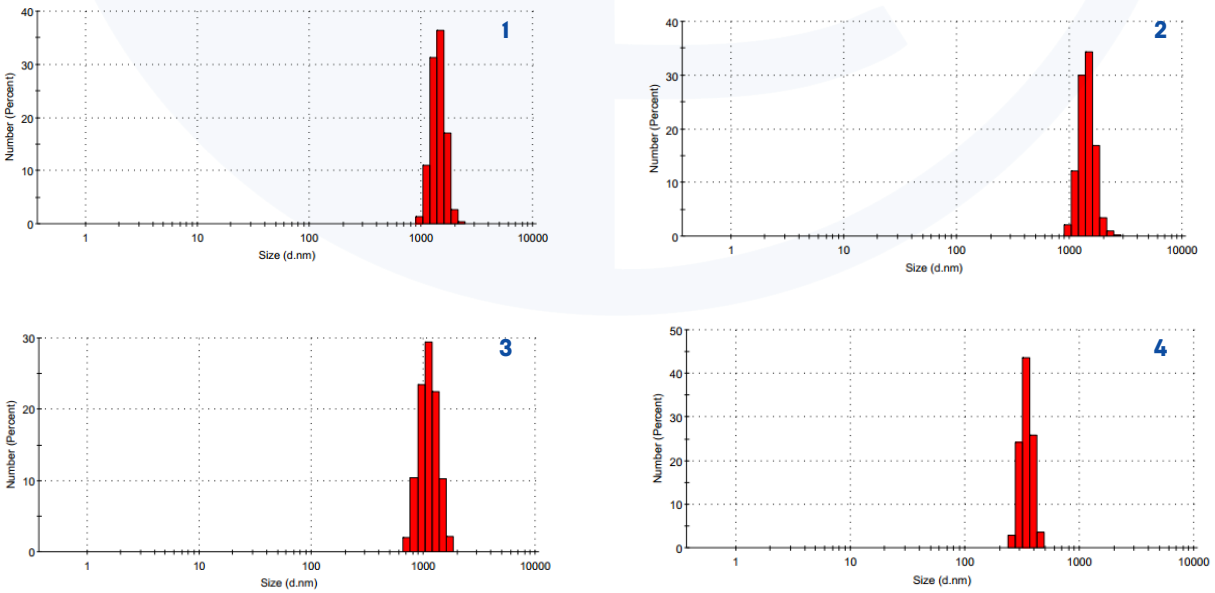

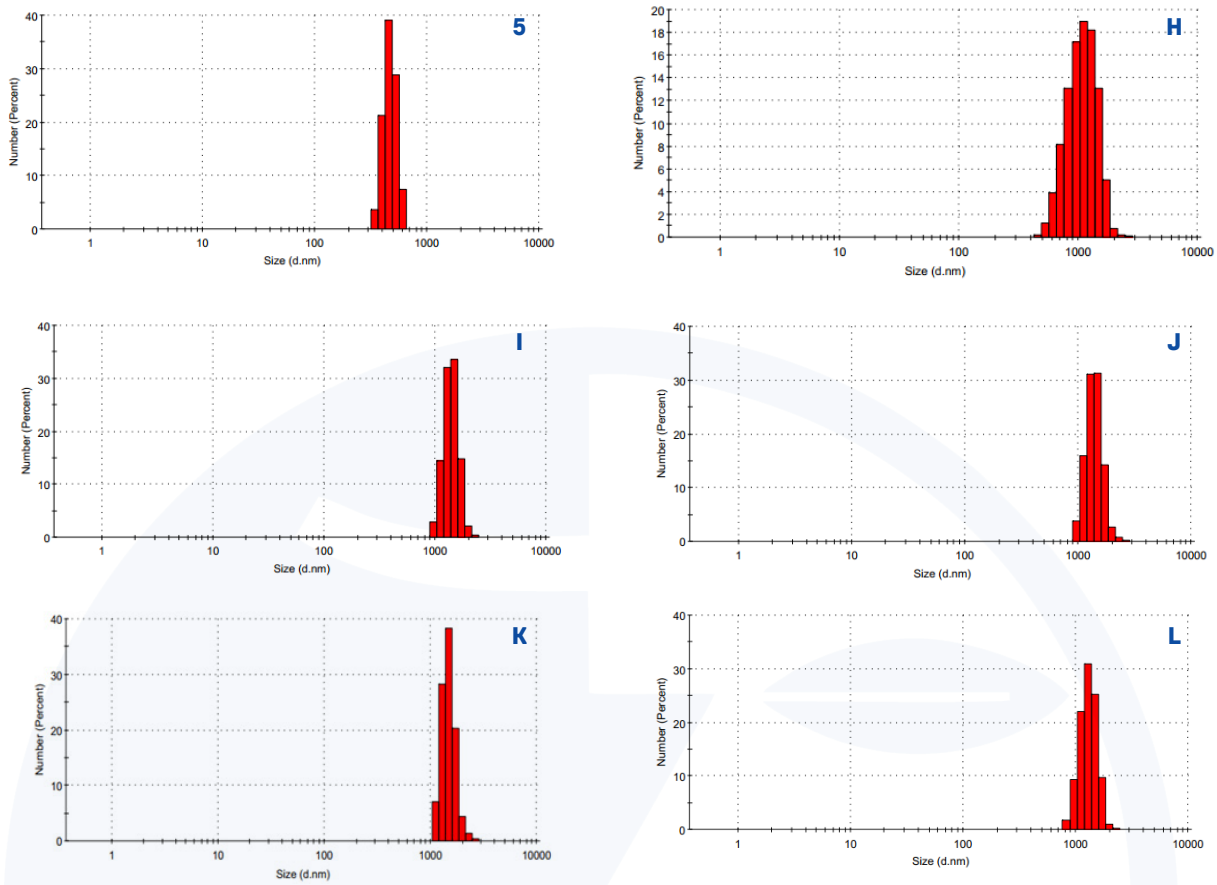

Figure 3 - The particle size distribution histograms from the DLS test for samples I, 2, 3, 4, and 5 (control) as well as samples H, I, J, K, and L (under the TCF)

According to the results shown in the histograms, it seems that samples (4) and (L) had the lowest and highest particle sizes, respectively. Also, the widest and narrowest particle size distributions were related to samples (H) and (4), respectively. The narrow particle size distribution means that the particle sizes were closer to each other and less different. For a more detailed study of the values obtained in this test, the parameters of mean and standard deviation were obtained and shown in Figure 4.

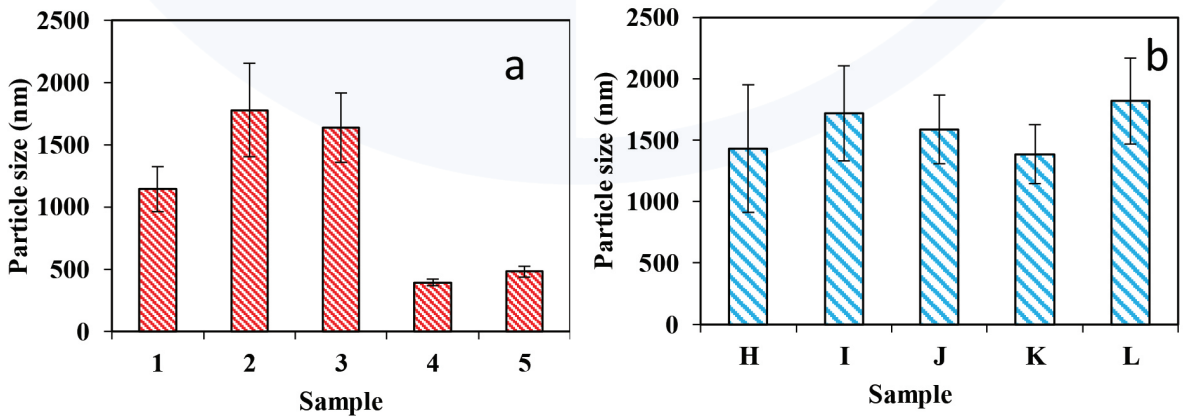

Figure 4- Changes in the mean particle size and standard deviation of the DLS test for samples of the control group (a), and samples under the TCF (b).

According to the results seen in Figure 4, the mean values in the sample (4) in the first group and sample (K) in the second group had the lowest values among the samples of each group. In addition, the largest particle size in the first group belonged to sample (2), and in the second group belonged to sample (L). It is also known that the average particle size in the samples under Consciousness Bond Field is larger than the first group. It is also clear that unlike the control group, where the difference in particle size with each other is relatively large (particle size range of about 400 to 1800 nm), in the group under the Consciousness Bond Field, the particles have almost similar sizes (particle size range of about 1400 to 1800).

Zeta Potential

The surface charge of a particle in a fluid is called zeta potential [10].

Zeta potential test is another method of evaluating the stability of nanoparticles in a suspension, the results of which can be related to the size of the hydrodynamic particles extracted from the DLS test. The results of this test are shown in Figure 5.

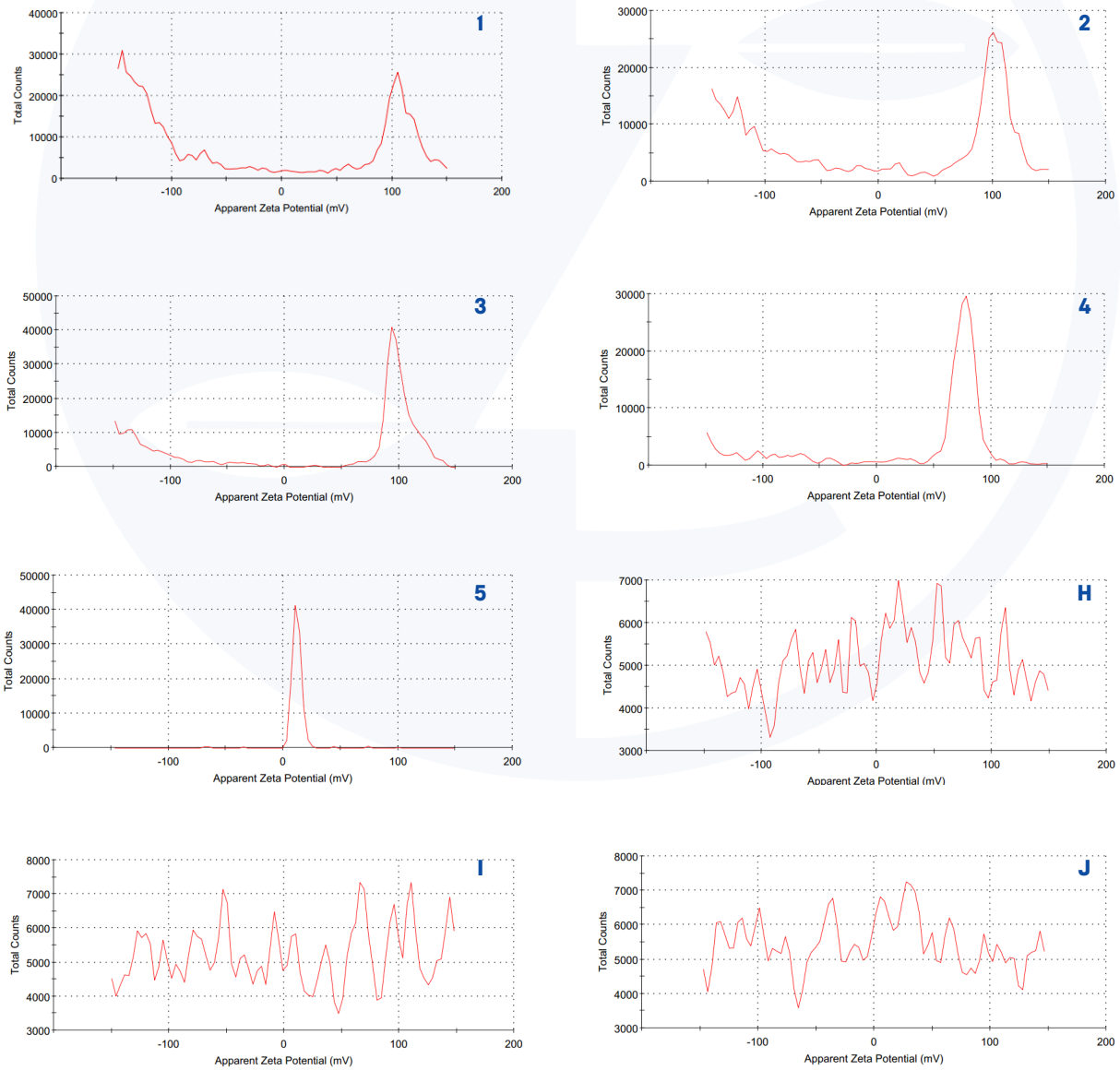

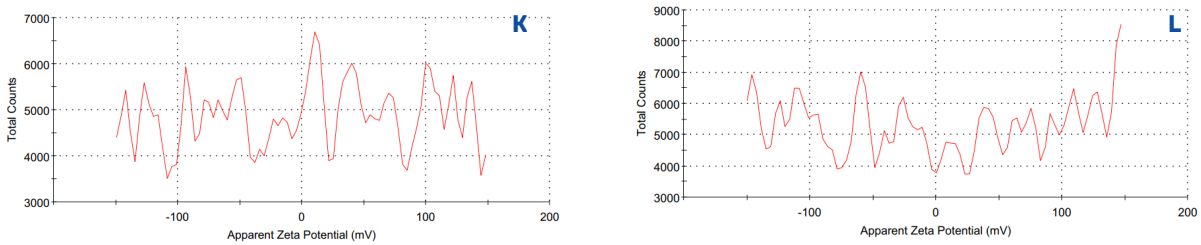

Figure 5- Zeta potential histogram of control samples 1,2,3,4,5 and samples H, I, J, K, L under TCF

According to these histograms, it is clear that all the graphs related to the group under the TCF are noisy, and these noises have caused the area under the curve in the whole histogram to move the mean value compared to the peak sharpness visible in the results. For this purpose, the mean value of the zeta potential is calculated and the bar graphs related to this parameter for different samples are shown in Figure 6.

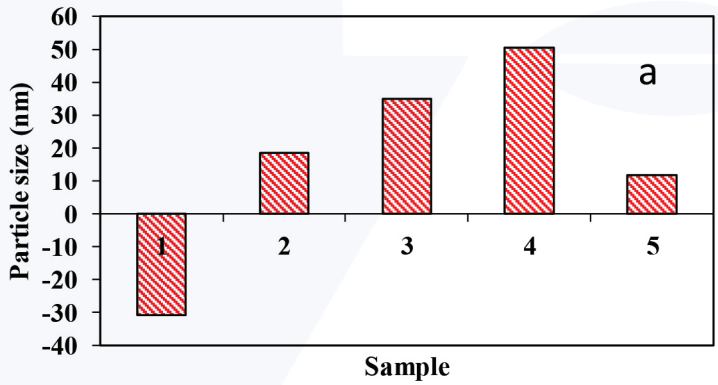

Figure 6- Changes in the mean value of the zeta potential for samples (a), the group as the control

It has been proven that the tendency of particles to repel each other is directly related to the zeta potential and, therefore, the boundary between the stability and instability of the suspension can be determined in terms of zeta potential. It is stated that particles with a zeta potential of more than 30 mV or less than -30 mV are stable in the diffuser bed [8,9]. In fact, the zeta potential of more or less than ± 30 mV causes an electrostatic repulsion force between the particles in the suspension and leads to the stability of these particles. Therefore, according to the results shown in Figure 5 in the control group, samples (1), (3), and (4) can be stable in colloids. In other samples, especially under CF, the cause of excessive noise and probabilities must be considered.

Examining the results of zeta potential, the following can be mentioned:

Sometimes samples contain a variety of chemicals that are not completely homogeneous, and the residual material in solution shows different charges due to the application of an electric field, and scattering or so-called noise appears. Given the complete purity of the material, this assumption is not acceptable. The second assumption is the agglomeration and non-uniformity of the sample, which is not accepted due to the good results of DLS. The third hypothesis is the possibility of the presence of fine particles around larger particles that show their surface charge due to the electric field of each particle [10] and changes in different levels appear as scattering and noise.

To investigate this possibility, in addition to TEM and SEM tests, zeta-potential re-testing was done by applying a 50 Hz ultrasonic bath with a Bandelin device.

Zeta potential with ultrasonic 50 Hz for 5 hours.

The results of the zeta potential test are shown in Figure 7.

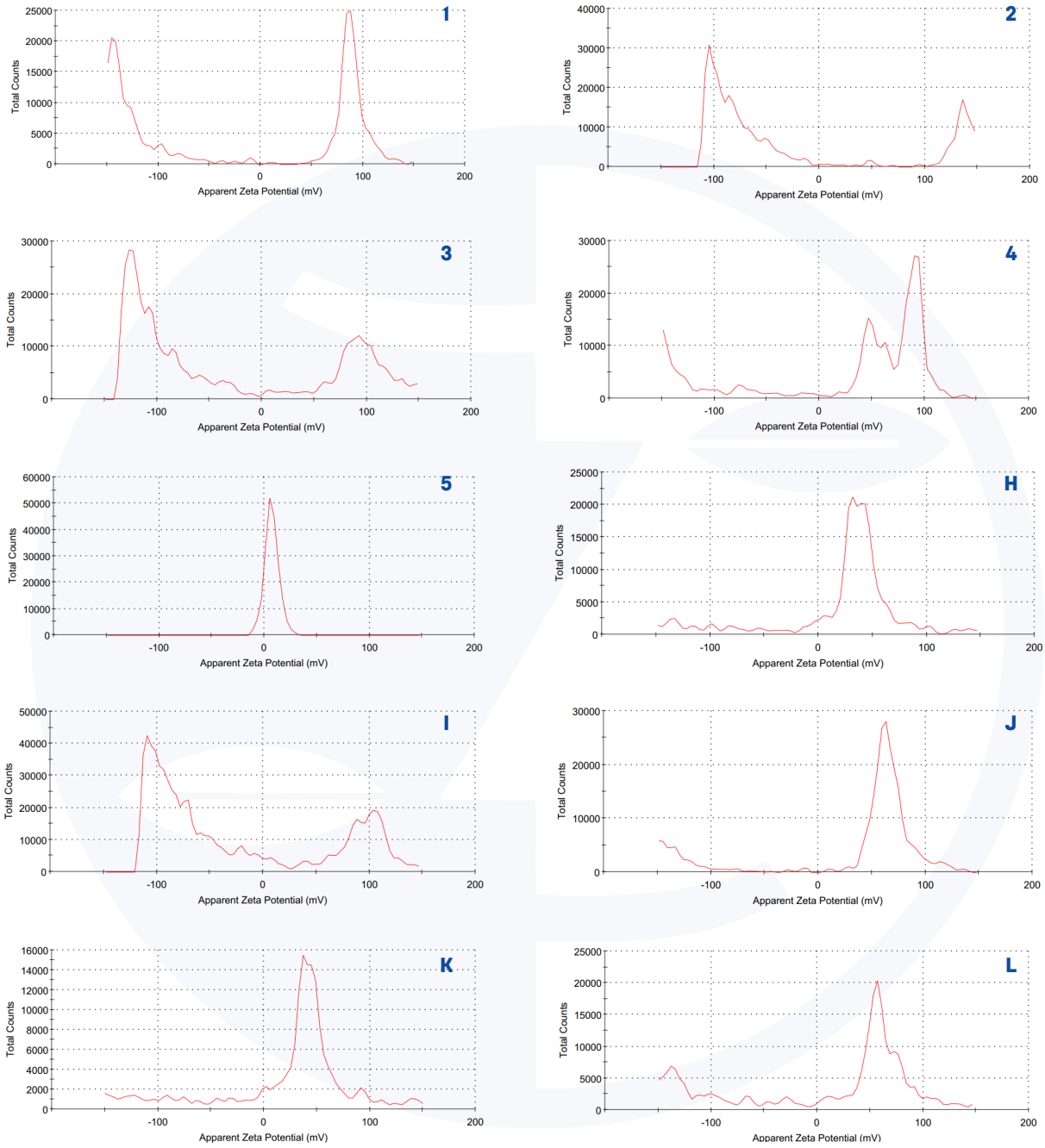

Figure 7- Zeta potential histogram of control samples I,2,3,4,5 and samples H, I, J, K, L under CF

According to these histograms, it is clear that except for samples (1) and (5) (and to some extent sample 4), the amount of zeta potential of the other samples has changed a lot compared to before. In the second group of samples (under the TCF) in particular, the spectrum of zeta potential changes is completely out of noise and scattering, and certain peaks can be observed in these spectra, which can increase the reliability of the results. The changes in the mean values of the zeta potential are plotted in Figure 8 in the form of bar graphs.

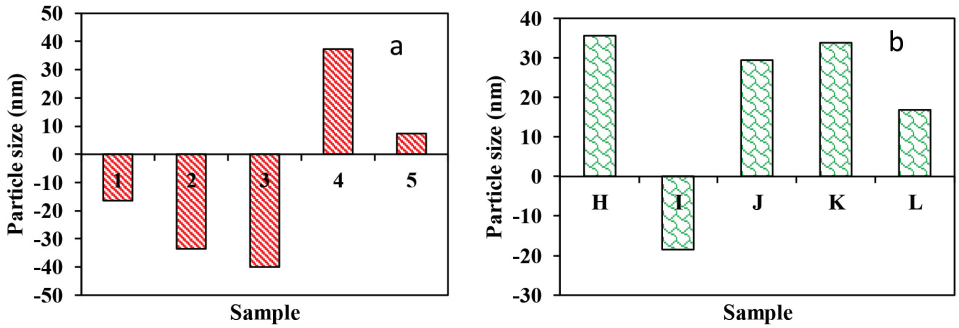

Figure 8- Changes in the mean value of the zeta potential for the control samples (a) and samples under TCF (b)

Therefore, according to the results shown in Figure 8 in the first group, samples (2, 3) and (4) can be stable in colloids. In the second group, samples (J, H) and (K) in the colloid can also be stable.

TEM (Transmission electron microscopy)

The results of the TEM test for the samples are shown in Figure 9.

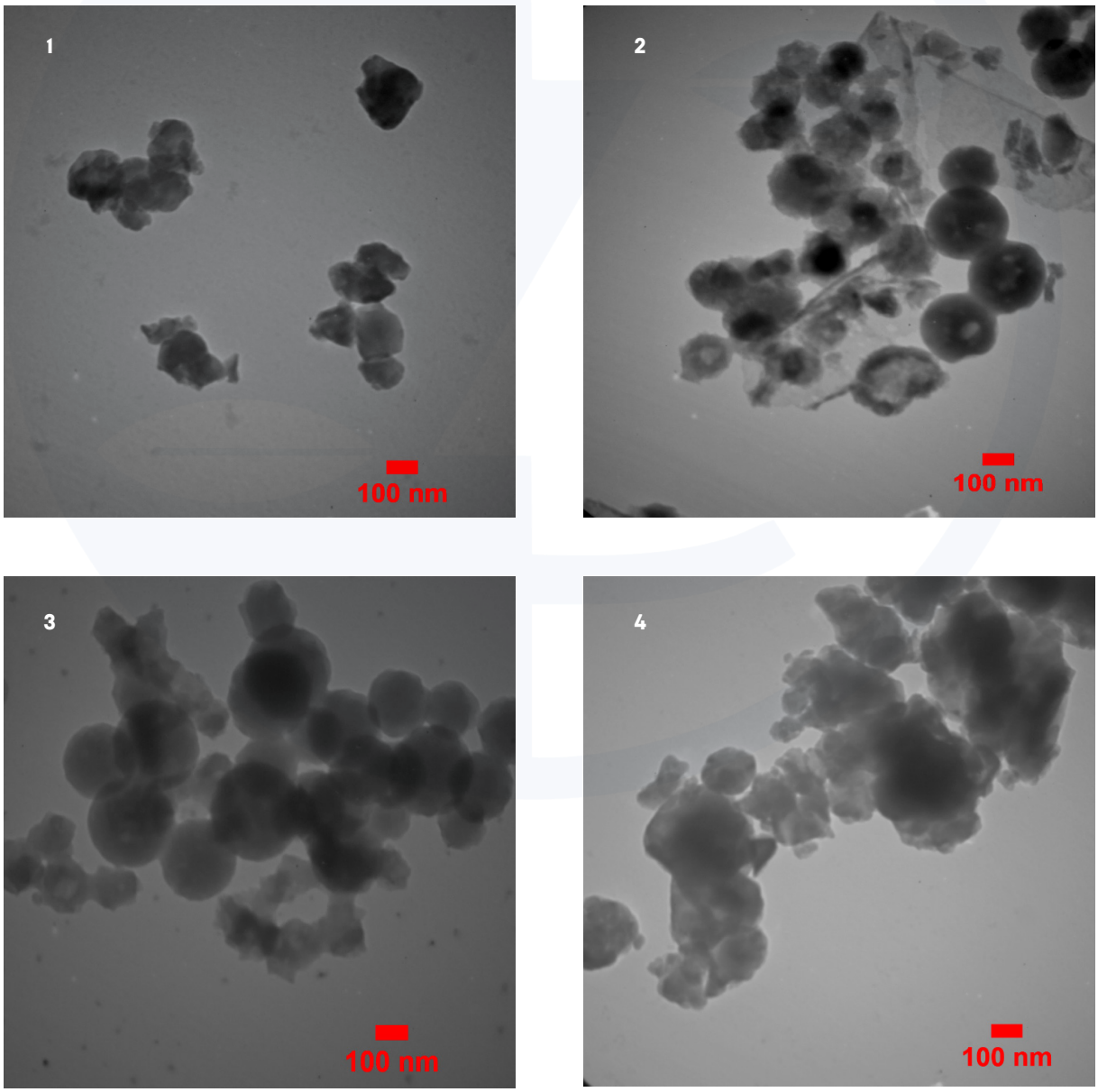

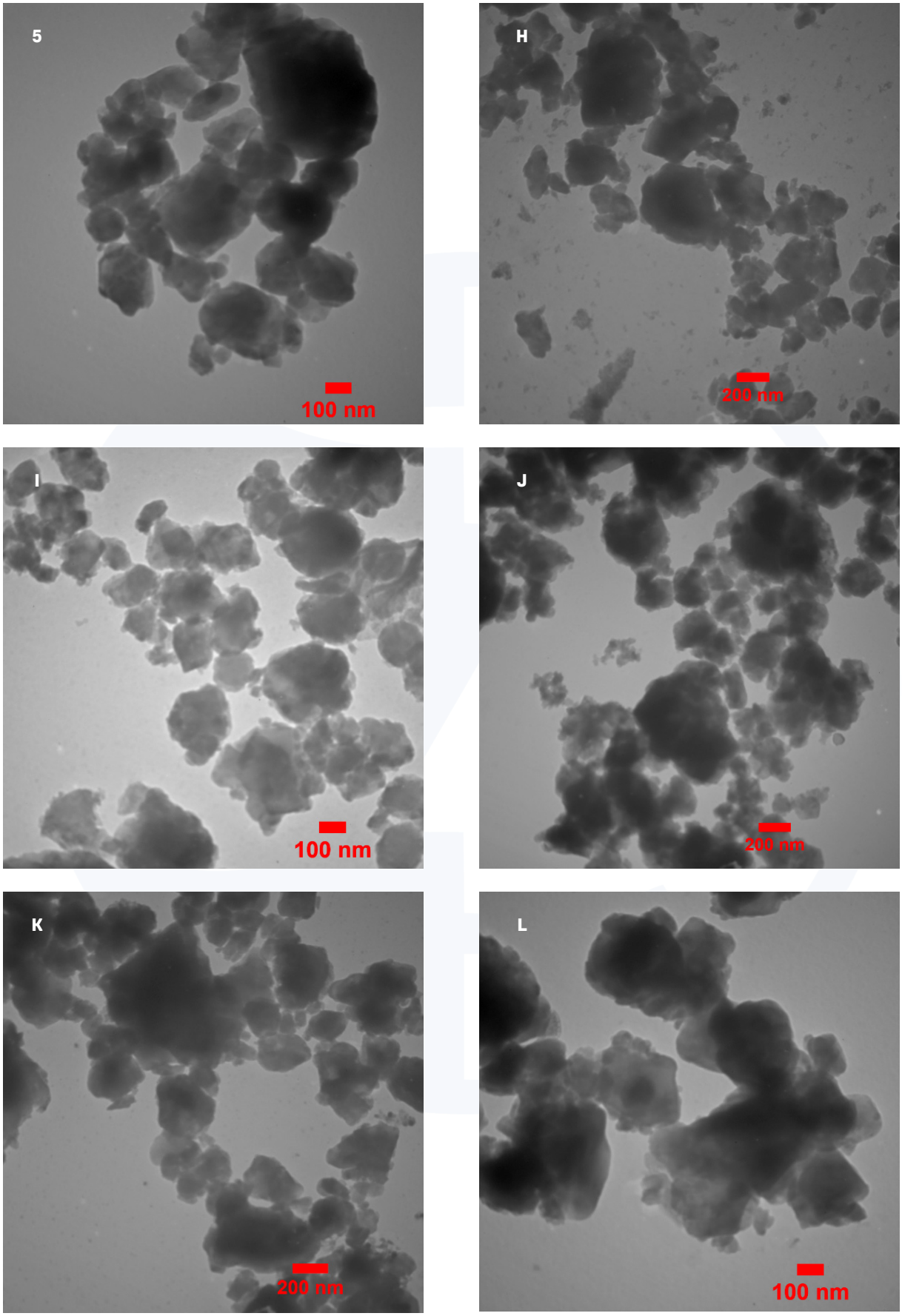

Figure 9- TEM test results for the control samples (1, 2, 3, 4, 5), and samples under TCF (H, I, J, K, L).

To check the particle size of each sample, in each sample, 50 particles of TEM images were measured by J-image processing software, and the histograms obtained from this measurement are shown in Figure 10.

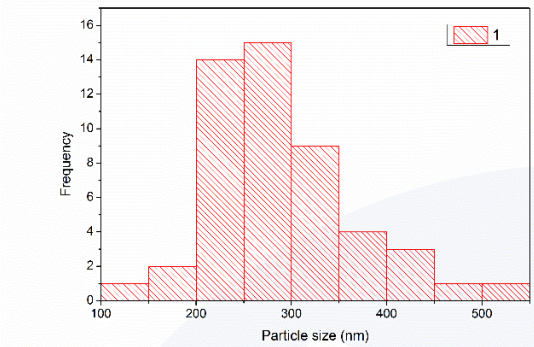

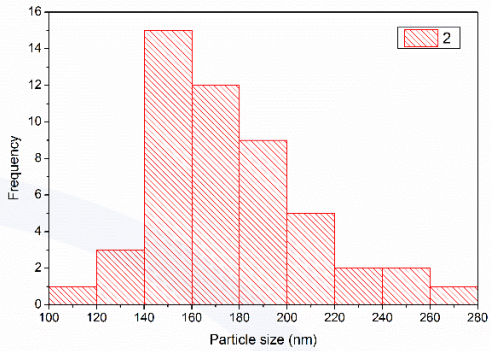

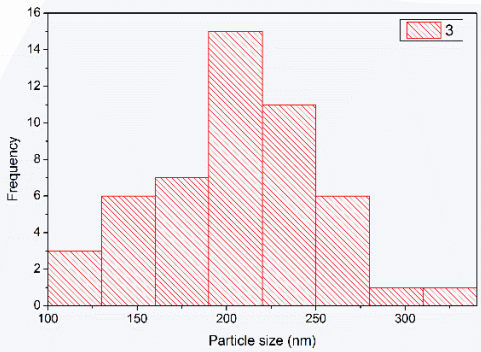

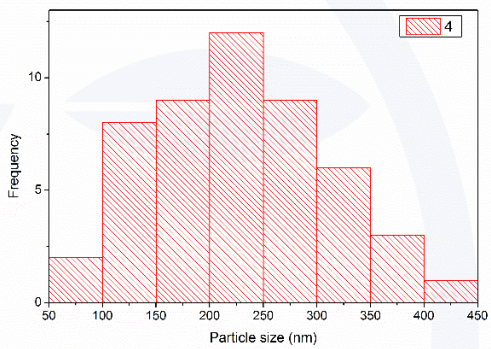

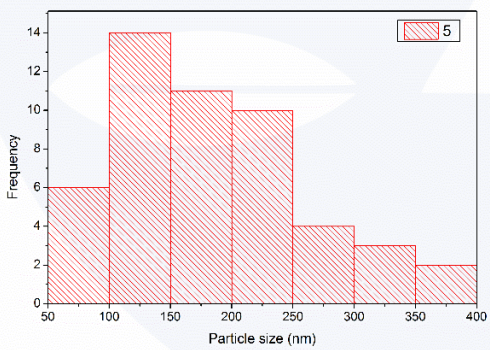

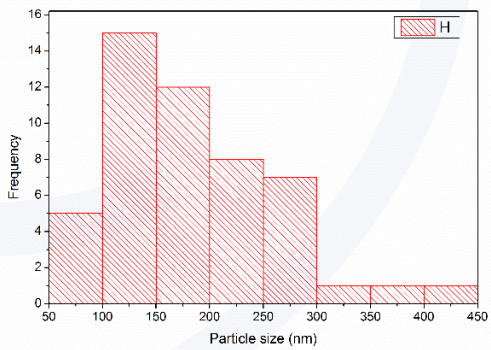

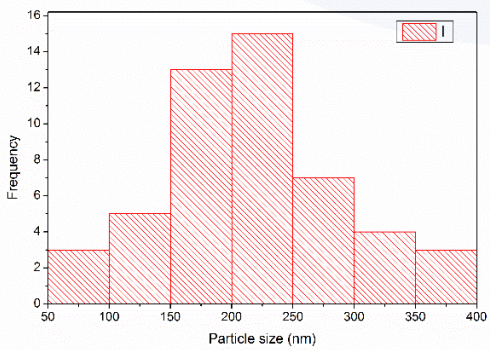

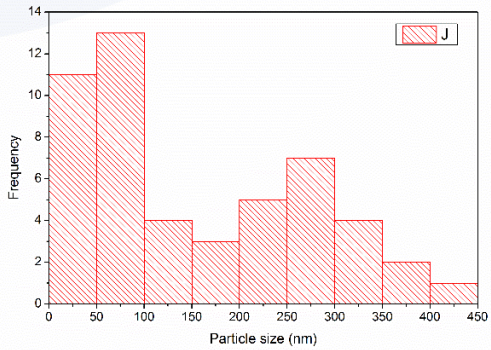

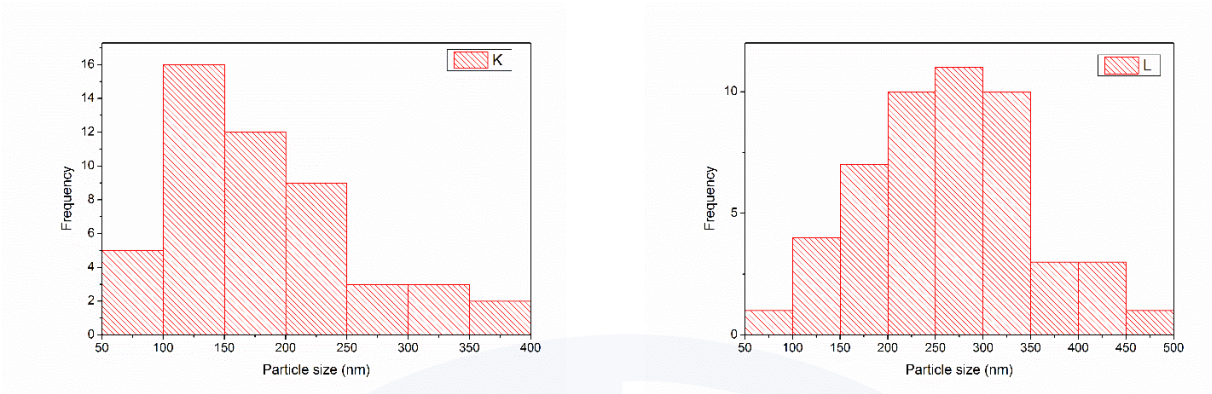

Figure 10. Histograms obtained by measuring 50 particles from TEM images related to the control samples (1, 2, 3, 4, 5) and the samples under TCF (H, I, J, K, L)

In these histograms, the horizontal axis is the particle size visible in the TEM images and the vertical axis is the number of particles in which the size range is measured by the software. According to the histograms shown in Figure 10, samples (2) and (J) have the narrowest and widest particle size distributions among the samples, respectively. The narrower the particle size distribution, the closer the particles are to each other, and the wider the particle size distribution, the greater the dispersion of the particle size. Other statistical data related to these measurements are reported in Table 4.

Table 4 . Statistical results from the histograms shown in Figure 10.(Control:1,2,3,4,5)&(TCF:H,I,J,K,L)

Sample	Total number of measurements	Mean (Nanometer)	Standard Deviation (Nanometer)	The smallest particle measured (Nanometer)	Measured sample of medium size (Nanometer)	The largest particle measured (Nanometer)
1	50	294.275	76.963	124.771	283.157	504.700
2	50	176.490	34.226	119.333	174.736	261.730
3	50	209.651	44.836	111.838	212.380	320.890
4	50	227.927	84.845	72.436	221.069	443.619
5	50	186.313	80.463	60.668	167.222	392.542
H	50	185.204	78.303	51.006	168.416	412.436
I	50	217.043	74.034	73.734	210.109	390.332
J	50	157.702	117.714	21.831	110.381	411.131
K	50	183.782	76.322	76.829	167.566	367.857
L	50	262.849	90.974	89.964	265.292	465.870

For easier examination and comparison of the mean and standard deviation values reported in Table 4, these values are plotted as bar graphs in Figure 11.

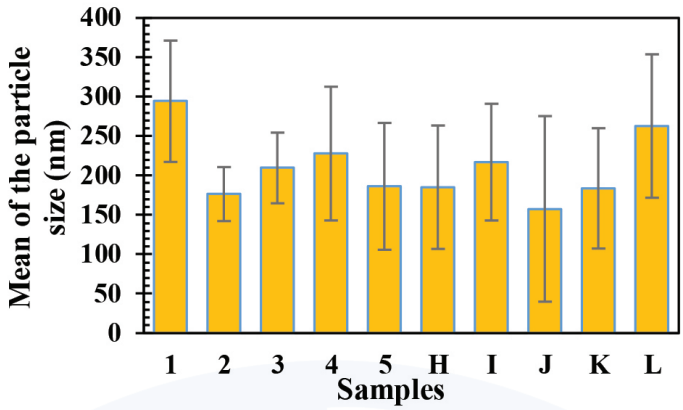

Figure 11- Particle size means and standard deviation of the samples. (Control:1,2,3,4,5) & (TCF:H,I,J, K, L)

According to Figure 11, samples (J) and (2) with particle size mean of 157.7 and 176.5 nm have the lowest particle size mean, followed by samples (K, H) and (5) with sizes of 183.8, 185.2, and 186.3 nm. It is also known that sample (1) with the particle size mean of 294.3 nm had the highest particle size among the samples, followed by sample (L) with the particle size mean of 262.6 nm and sample (4) with the particle size mean of 227.9 nm.

SEM (Scanning Electron Microscopy)

The images related to the samples were presented below (figure 12-21).

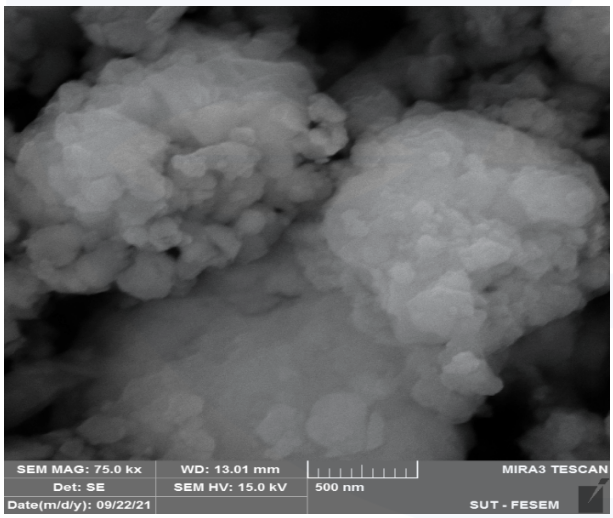

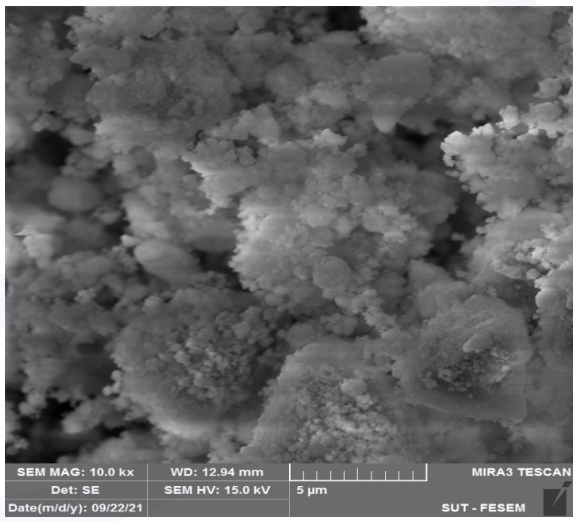

Element	Line Type	Apparent Concentration	k Ratio	Wt%	Wt% Sigma	Atomic %	Standard Label	Factory Standard
O	K series	13.75	0.04627	53.44	0.20	67.00	SiO2	Yes
Si	K series	11.25	0.08911	45.85	0.19	32.74	SiO2	Yes
Fe	K series	0.13	0.00133	0.71	0.12	0.25	Fe	Yes
Total:				100.00		100.00		

Figure 12- Sample I (Control)

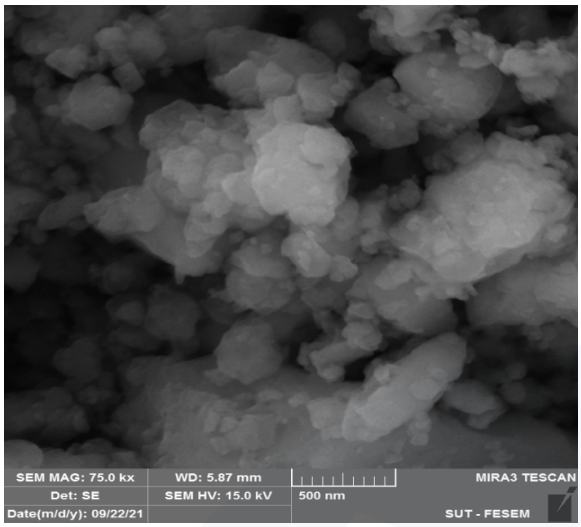

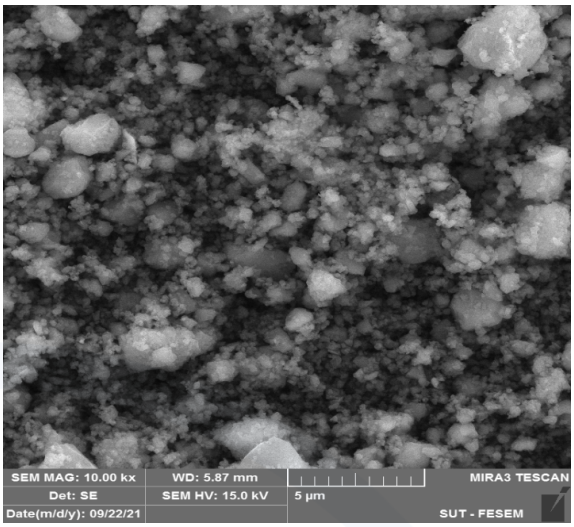

Element	Line Type	Apparent Concentration	k Ratio	Wt%	Wt% Sigma	Atomic %	Standard Label	Factory Standard
O	K series	14.60	0.04914	53.41	0.20	67.02	SiO2	Yes
Si	K series	11.88	0.09414	45.68	0.19	32.65	SiO2	Yes
Fe	K series	0.18	0.00180	0.90	0.12	0.32	Fe	Yes
Total:				100.00		100.00		

Figure 13- Sample 2 (Control)

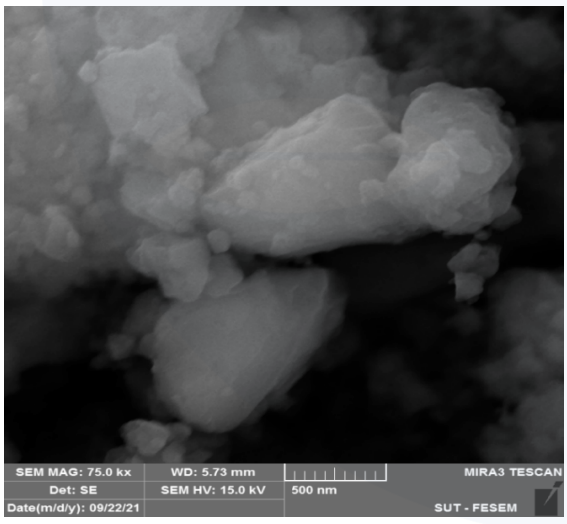

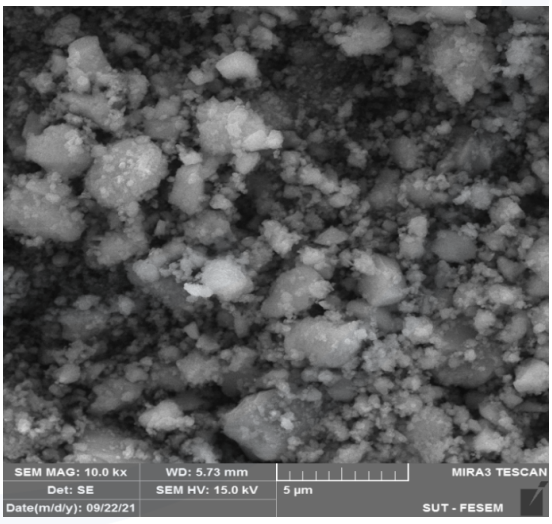

Element	Line Type	Apparent Concentration	k Ratio	Wt%	Wt% Sigma	Atomic %	Standard Label	Factory Standard
O	K series	7.20	0.02423	46.60	0.21	60.92	SiO2	Yes
Si	K series	8.24	0.06527	51.54	0.21	38.38	SiO2	Yes
Fe	K series	0.22	0.00225	1.86	0.16	0.69	Fe	Yes
Total:				100.00		100.00		

Figure 14- Sample 3 (Control)

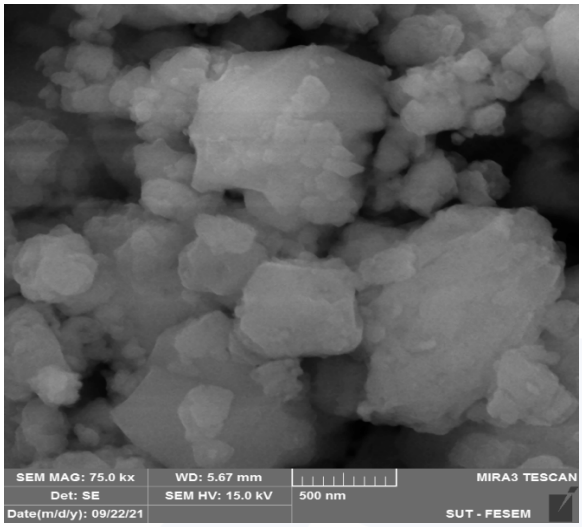

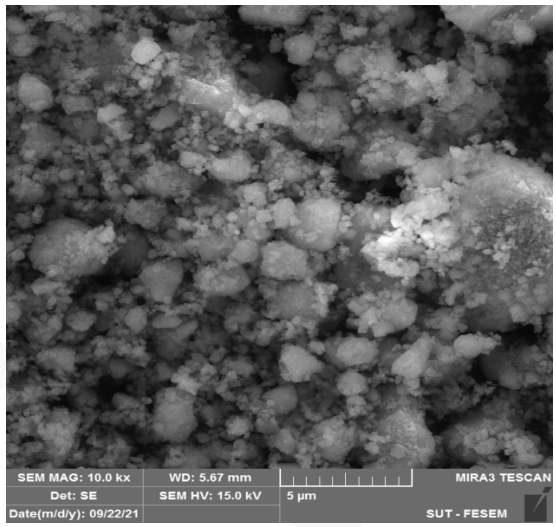

Element	Line Type	Apparent Concentration	k Ratio	Wt%	Wt% Sigma	Atomic %	Standard Label	Factory Standard
O	K series	12.50	0.04206	51.29	0.20	65.15	SiO2	Yes
Si	K series	11.36	0.09002	47.64	0.20	34.47	SiO2	Yes
Fe	K series	0.19	0.00193	1.07	0.13	0.39	Fe	Yes
Total:				100.00		100.00		

Figure 15- Sample 4 (Control)

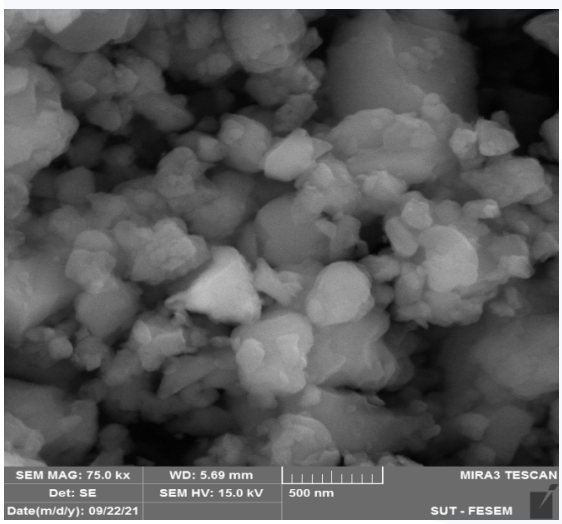

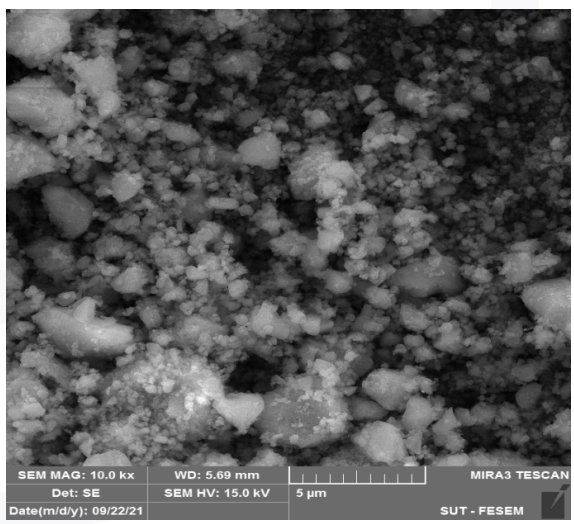

Element	Line Type	Apparent Concentration	k Ratio	Wt%	Wt% Sigma	Atomic %	Standard Label	Factory Standard
O	K series	9.39	0.03159	48.38	0.21	62.39	SiO2	Yes
Si	K series	10.09	0.07993	50.79	0.21	37.31	SiO2	Yes
Fe	K series	0.12	0.00124	0.83	0.14	0.31	Fe	Yes
Total:				100.00		100.00		

Figure 16- Sample 5 (Control)

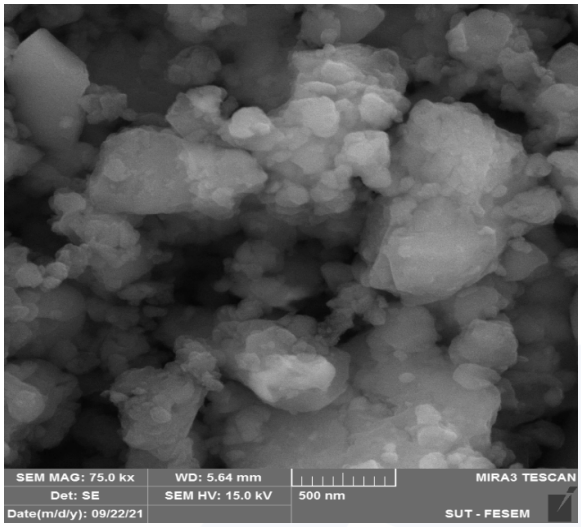

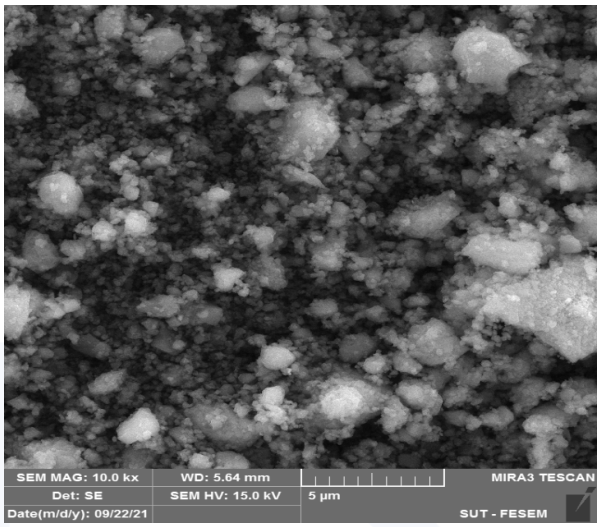

Element	Line Type	Apparent Concentration	k Ratio	Wt%	Wt% Sigma	Atomic %	Standard Label	Factory Standard
O	K series	17.94	0.06038	54.03	0.19	67.57	SiO2	Yes
Si	K series	14.12	0.11187	45.09	0.19	32.12	SiO2	Yes
Fe	K series	0.21	0.00211	0.88	0.12	0.32	Fe	Yes
Total:				100.00		100.00		

Figure 17- Sample H (under TCF)

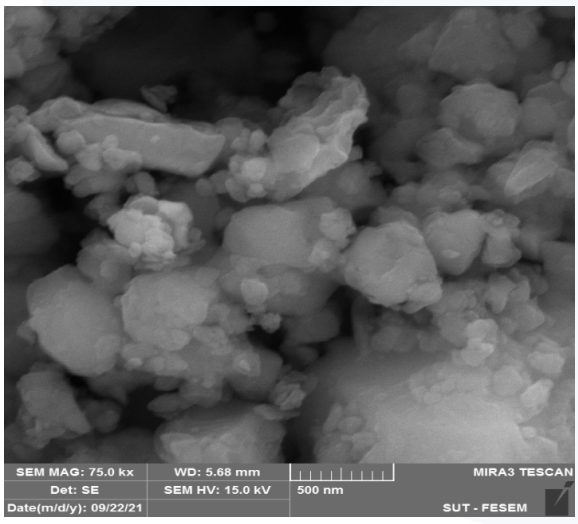

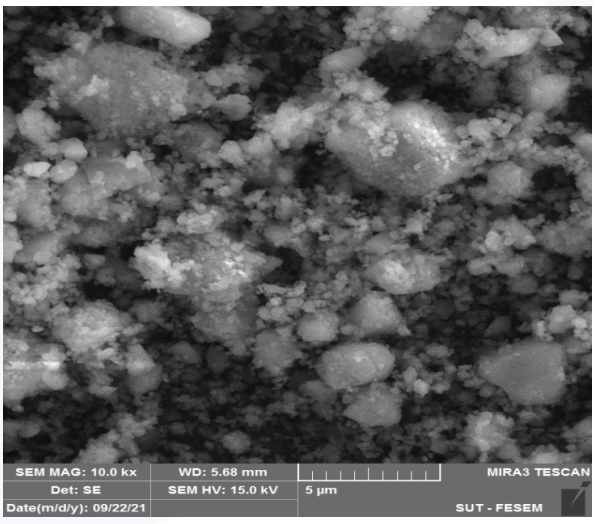

Element	Line Type	Apparent Concentration	k Ratio	Wt%	Wt% Sigma	Atomic %	Standard Label	Factory Standard
O	K series	15.07	0.05071	51.97	0.20	65.80	SiO2	Yes
Si	K series	13.12	0.10395	46.80	0.19	33.75	SiO2	Yes
Fe	K series	0.26	0.00262	1.23	0.13	0.44	Fe	Yes
Total:				100.00		100.00		

Figure 18- Sample I (under TCF)

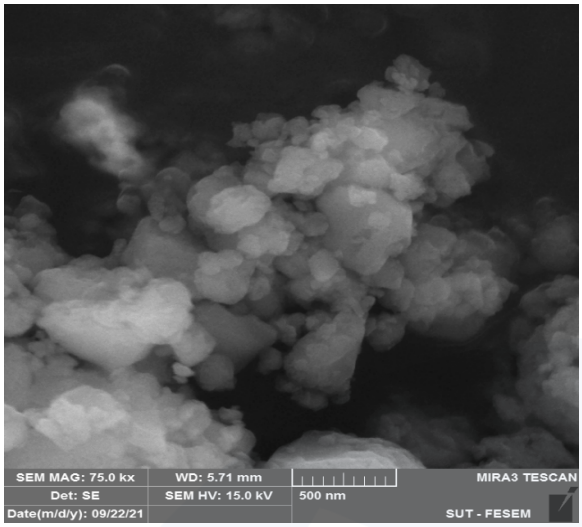

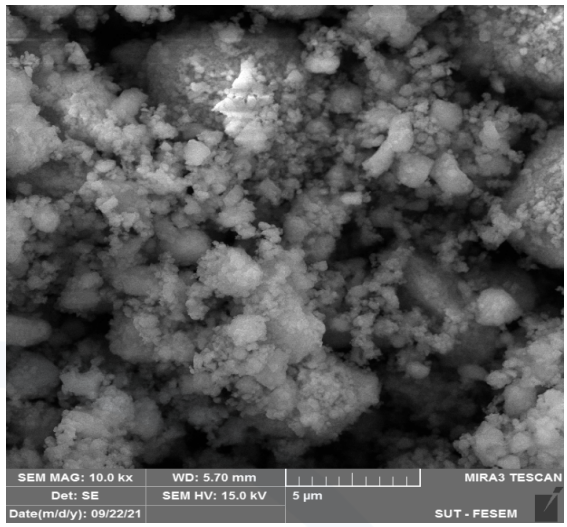

Element	Line Type	Apparent Concentration	k Ratio	Wt%	Wt% Sigma	Atomic %	Standard Label	Factory Standard
O	K series	16.70	0.05620	53.01	0.20	66.70	SiO2	Yes
Si	K series	13.80	0.10937	45.91	0.19	32.91	SiO2	Yes
Fe	K series	0.25	0.00249	1.09	0.12	0.39	Fe	Yes
Total:				100.00		100.00		

Figure 19- Sample J (under TCF)

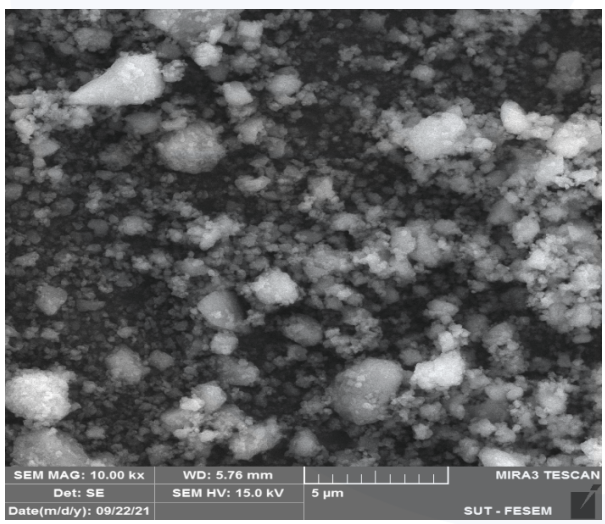

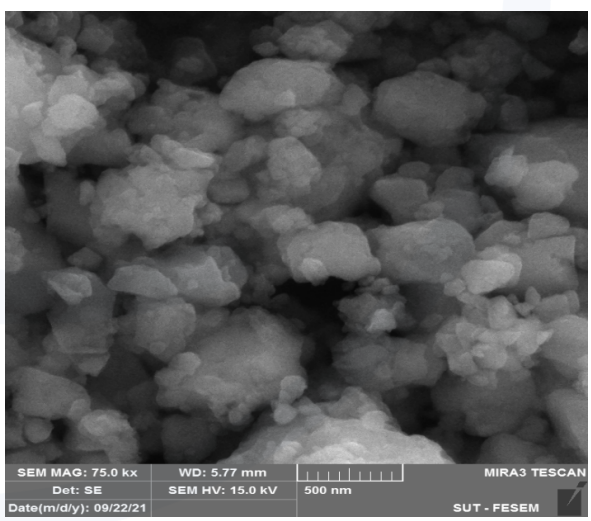

Element	Line Type	Apparent Concentration	k Ratio	Wt%	Wt% Sigma	Atomic %	Standard Label	Factory Standard
O	K series	19.83	0.06672	55.92	0.19	69.15	SiO2	Yes
Si	K series	14.21	0.11259	43.51	0.18	30.65	SiO2	Yes
Fe	K series	0.14	0.00141	0.56	0.11	0.20	Fe	Yes
Total:				100.00		100.00		

Figure 20- Sample K (under TCF)

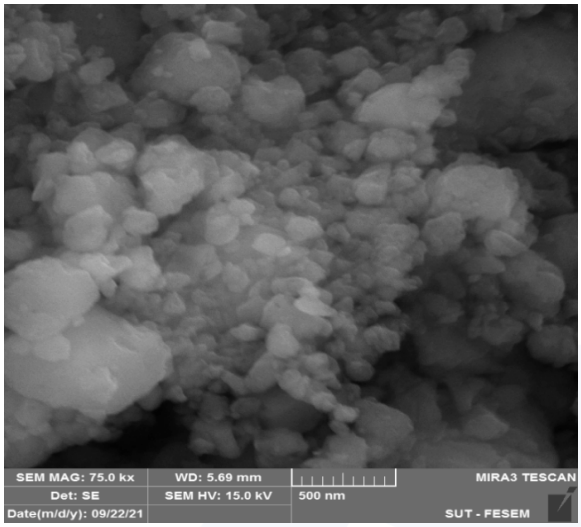

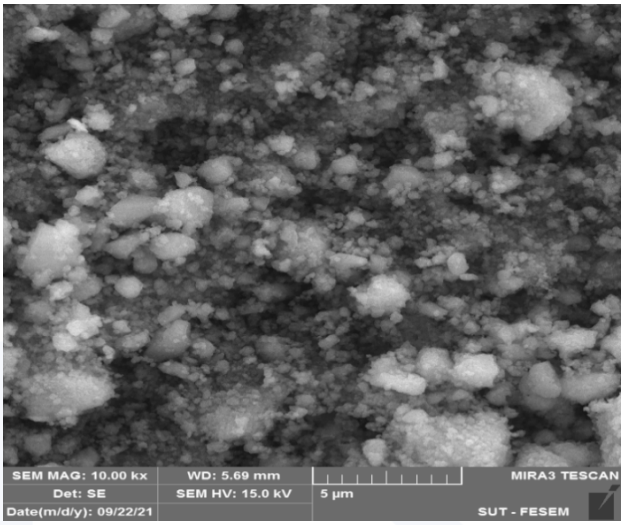

Element	Line Type	Apparent Concentration	k Ratio	Wt%	Wt% Sigma	Atomic %	Standard Label	Factory Standard
O	K series	8.28	0.02787	45.69	0.22	59.87	SiO2	Yes
Si	K series	10.20	0.08081	53.18	0.22	39.70	SiO2	Yes
Fe	K series	0.16	0.00165	1.14	0.15	0.43	Fe	Yes
Total:				100.00		100.00		

Figure 21- Sample L (under TCF)

Vol. 01
No. 06
April
2022
139
The First Journal in T-Consciousness Research

Conclusion

Milling pure silica under T-Consciousness Bond Field had the following results:

1- Since the material used was silica with 98% purity and pure materials remain pure in the variable T-Consciousness Field, Consciousness Bond Field in this study, so only the silica oxide was still seen in the X-ray diffraction results [11]. The parameters related to the crystal structure remained constant under the TCF and only micro-strain differences were observed. The distortion and stress in the crystal grid structure under the TCF were much less (about 80%).

2- In the particle size distribution and the amount of hydrodynamic particle size, it was found that the dispersion in the samples under T-Consciousness Bond Field was less and the structure was more uniform. Particle size dispersion was obtained at 400 to 1800 nm in control samples and 1400 to 1800 nm in samples under T-Consciousness Bond Field. Particle sizes in the high dimension range were in the majority.

3- TEM analysis and SEM images, show that the size of the smallest particles in the T-Consciousness Bond Field is smaller (~35.9%) and often the dispersion of fine particles is increased in the empty space between the larger particles.

4- One of the occurrences is the high dispersion zeta potential diagrams under the TCF. Finally, it is impossible to study the zeta potential in the TCF, and so-called so much noise is generated that the output of the voltage is eventually estimated to be zero. The causes of

this dispersion can be due to several reasons:

Chemical compounds that do not react completely and are still present in the material and cause different ionic rings, which is also not possible with the purity of the material.

Having different particle dimensions and polydispressing of the material, the ionic ring of each particle is different and is seen in the form of noise in interference. This is different from the DLS test because the results show that the maximum statistical population is more uniform.

The ultimate reason is the possibility of creating particles with dispersed dimensions and charge differences, which with a hypothesis of electric charge variation, their surface is high, which ultimately does not create a relative equilibrium and peak sharp, but their number is not large enough to affect the DLS test. To investigate this possibility, the zeta potential test was performed with the previous conditions but by placing the particles in an ultrasonic bath. Ultra-sonication of the particles meant that not all of the particles were completely disintegrated into agglomerates and that whatever was present on the surface of the particles could be received. In the re-test, and especially by examining the results of the control sample, it is clear that the sample particles are completely disintegrated and the variation of the electric charge of the particle surface is in relative equilibrium. Therefore, by examining these results, it is clear that the diversity of particles in the sample under TCF is not necessarily the cause of the diversity of electrical charges. And one of the effects that TCF has on the matter in the short run is the interference with the electric charge of the surfaces of the particles. Although the dimensions and reasons for this still require extensive experiments, in the first impression it can be said that since consciousness has the ability to become matter and energy, it can affect the speed of particle motion and cause apparent dispersion.

References

1- EU (European Union). (2011). 696.EU

2- Taheri, M. A. (2013). *Human from another outlook.* Interuniversal Press. 2nd Edition. ISBN-13: 978-1939507006, ISBN-10: 193950700

3- Taheri, M. A. (2012). *General Connection of particles.* Interuniversal Publishing.Erfan-Hlgheh. ID: 978-1-940491-03-5.

4- Kazazi, B, Taheri. M. A, Meshkin-Far. A. (2020). Influence of the Consciousness Field on the Cement Properties and Behavior. Science of Consciousness, Tucson, Arizona

5- Taheri, M. A. (2020). The main monitoring center for T-Consciousness Fields research and studies based on Sciencefact. www.Cosmointel.com.

6- Hernandez. C.C, Ferreira .F. F, Rosa. D. S. (2018). X-ray powder diffraction and other analyses of cellulose nanocrystals obtained from corn straw by chemical treatments. Carbohydr Polym;193:39–44. https://doi.org/10.1016/j.carbpol.2018.03.08

7. Ju. X, Bowden M, Brown E E, Zhang X.(2015). An improved X-ray diffraction method for cellulose crystallinity measurement. Carbohydr Polym 123:476–81. https://doi.org/10.1016/j.carbpol.2014.12.071

8- Bhattacharjee. S. (2016). DLS and zeta potential – What they are and what they are not? J. Control. Release. 235 .337–351. https://doi.org/10.1016/J.JCONREL.2016.06.017.

9- Honary. S, Zahir .F. (2013). Effect of Zeta Potential on the Properties of Nano-Drug Delivery Systems- A Review (Part 1),Trop. J. Pharm. Res. 12 .255–264. https://doi.org/10.4314/tjpr.v12i2.19.

10- Kaszuba .M, Corbett .J, Watson .F.M, Jones .A.(2010). High-concentration zeta potential measurements using light-scattering techniques Philos. *Transact. A Math. Phys. Eng. Sci.* 368 4439–4451.

11- Kazazi. B, Taheri. M. A. (2021). Effect of the Consciousness Bond Field on the structure and properties of Aluminum .www.cosmointel.com